Synthesis, Characterization of Gd-doped Ceria Nanocomposites

Dr. M.J. Pawar[a]*, Sagar B. Deshmukh[a], Dr. Shrikant D. Thakre[b], Dr. Anand S. Tale[c]

[a] *Department of Chemistry, Laboratory of Material Synthesis, Smt. Narsamma Arts, Commerce and Science College, Kiran Nagar, Amravati (MS).*

[b]*Dr. Rajendra Gode Institute of Technology & Research, Amravati (MS),*

[c] *Shri Sant Gajanan Maharaj College of Engineering, Shegaon (MS).*

Abstract

In this work, Gd-doped CeO_2 ($Ce_{1-x}Gd_xO_{2-\delta}$; x = 0.0. 2.0, 4.0 and 6.0 wt %) nanocomposites were prepared by EDTA-Glycol method. The influence of Gd doping on the microstructures and the optical and ionic conductivity properties of these nanoparticles has been studied using X-ray diffraction, FTIR, TEM, UV-VIS, SEM-EDS and impedance spectroscopy. It has been found that Gd doping formed a homogeneous solid solution with ceria, with a significative reduction of crystallite size. As compared to the pure ceria an improvement of total conductivity was achieved with a maximum for the highest Gd concentration of 4 wt % in the temperature range of 550–950°C.

1. Introduction

Solid oxide fuel cell (SOFC) is one of the most promising electrochemical devices for clean power generation due to its efficient operation, fuel flexibility (ranging from hydrogen to hydrocarbons and biogas), and relatively lower greenhouse gas emissions [1,2]. Comparable to other types of fuel cells, SOFCs have the advantage of fuel flexibility i.e. are able to work with hydrogen, hydrocarbon reformate and, in some conditions, with hydrocarbon fuels directly [3-5]. Furthermore, SOFCs are highly promising due to their enhanced resistance to fuel contamination and versatility of applicable combustible gases in comparison with other FC types. Presently, solid electrolytes for SOFCs working in medium temperature region (400–800°C) often comprise cerium oxide doped with rare earth oxides [6,7]. Ceria-based electrolytes possess an advantageous combination of high unipolar oxygen

conductivity, chemical stability in carbon- and hydrogen-containing atmospheres and an inertness to electrode materials, which makes them highly promising for medium-temperature fuel cells.

Being comparable with conventionally used zirconia with respect to electric performances, CeO_2-based electrolyte nanomaterials allow for a significant reduction of working temperature for fuel cells, thus providing an increased durability and simplified structure [8,9].

In addition, doped ceria-based electrolyte materials, such as gadolinium-doped ceria (GDC) or samarium-doped ceria, exhibiting an ionic conductivity than YSZ in the temperature range of 600–750°C [10]. However, the functional limitation of doped ceria-based electrolytes is that they exhibit appreciable electronic conductivity at higher temperature (≥ 800°C) and low partial pressure of oxygen at anode side that dictates the operating temperature of the fuel cells [11–15].

Many methods including ultra-sonication, ball milling, microwave, sol–gel, mechanical alloying and chemical-precipitation, etc. for the preparation of nanocomposite materials from the mixed metal oxide precursors. [15-17]. From above all well-known methods, the chemical-precipitation process is used as a competent technique for the production of nanomaterials, owing to effortlessness. This move toward is extra operative for yielding homogeneity, particularly sample without impurities, tiny particle size, and a short period of time. Ceria-based materials are serious candidates with samarium [18-20] or gadolinium [21-25] substitution to increase the vacancy concentration.

In doped ceria, it has been reported that when the dopant ion radius is close to the critical radius (1.038 Å), then the doped ceria exhibits the highest oxygen ion conductivity. For this reason, Gd doped ceria exhibits the highest oxygen ion conductivity among the doped ceria, as radius of Gd^{3+} (1.05 Å) is closer to the critical radius (1.038 Å) [26, 27]. However, the exact composition of CeO_2-Gd_2O_3 system that has maximum oxygen ion conductivity is still not well defined. *Mori* et al. [28, 29] showed the domain structure in rare earth doped ceria grains and suspected that these domains present in grains are responsible for the higher grain conductivity of $Ce_{0.9}Gd_{0.1}O_{2-\delta}$. But, *Kharton* et al. [30] reported the higher total conductivity for $Ce_{0.2}Gd_{0.2}O_{2-\delta}$ which was possibly due to a contribution of grain boundary conductivity. Moreover, although the Gd_2O_3-CeO_2 system has been reported by several authors, few works provide a comprehensive microstructural and electrical analysis of 0, 10 and 20 mol% Gd_2O_3-doped CeO_2, formed by such low temperature, soft chemical preparation routes. In this work, we synthesized $Ce_{1-x}Gd_xO_{2-d}$ (x = 0, 0.1 and 0.2) nanoparticles by

the sol gel combustion route for intermediate temperature electrochemical applications. The synthesized materials are fully characterized by their structural, chemical, microstructural and electrical properties. Gd doped ceria synthesized by solid-state reaction requires high sintering temperature and time. Hence various wet chemical methods have been used for the synthesis Gd doped ceria such as co-precipitation [31], combustion [32, 33], sol-gel [34, 35], hydrothermal [36], EDTA-citrate complexation [37] and micro-emulsion [38]. To the best our knowledge, no reports are available on synthesis of Gd doped ceria by EDTA-Glycol complexation method. Hence in this investigation, we present a systematic study of effect of pH on structural, morphological and electrical properties of Gd doped ceria solid solutions obtained by EDTA-Glycol method.

2. Experimental

2.1 Materials

In this work, for preparation of ceria based nanocomposites, highly pure $Ce(NO_3)_3.6H_2O$ and $Gd(NO_3)_3.6H_2O$ were use as the source of metal ions obtained from Sigma Aldrich. The other chemicals used in synthesis Nitric Acid (HNO_3, 65%, Merck), ethylene diamine tetra acetic acid ($C_{10}H_{16}N_2O_8$; Sigma Aldrich), ethylene glycol ($C_2H_6O_2$; Merck), were used as obtained without further purification.

2.2 Method of Synthesis

The pure and Gd doped CeO_2 materials were used by a modified EDTA-Glycol method [14]. The highly pure $Ce(NO_3)_3.6H_2O$, $Gd(NO_3)_3.6H_2O$ were used as the precursors. These salts were mixed independently in de-ionized water. During meanwhile 2, 4 and 6 wt % of gadolinium nitrate solution were added to the above reaction mixture and continuously stirred for 30 min. The calculated quantity of ethylenediaminetetraacetic acid (EDTA), dilute ammonia and ethylene glycol (EG) was added to the nitrate solution. So formed solution was stirred and kept on a hot plate for heat treatment at 80°C which in turn forms a gel-like mass. The resulted mass was combusted at 300°C for 2 h followed by the calcination at 550°C for 5 h. On calcinations, the obtained ashes were ground in agate mortar to get fine homogeneous powders. Powder materials were uniaxially pressed into pellets with

6 mm of diameter and 2 mm thickness, at 200 MPa. Sintering was performed in air for 10 h at a constant heating rate (CHR) of 2°C/min in between 1150°C to 1350°C.

3. Characterization

Calcined powders were studied by X-ray diffraction (XRD) using a Miniflex 600 diffractometer RIGAKU - Japan (Cu–$K\alpha$ radiation). Data in an angular region of 2θ in the range of 20-80° were collected in a step-scanning mode (0:02 steps with a step-counting time of 2 s). The crystallite size, D, of the calcined powders was estimated using the Scherrer equation:

$$D = \frac{0.9\lambda}{\beta cos\theta} \tag{3.1}$$

Where, D is crystallite size, λ is wavelength of X-rays (1.5418Å), θ is the scattering angle of the main reflection and β is the corrected peak at full width at half-maximum (FWHM) intensity. FTIR of the as-prepared samples were investigated by IR Affinity-1 Shimadzu- Japan. UV-visible spectra of the samples were studied by using UV–1800 Shimadzu- Japan. SEM-EDS studies was performed on Carl Zeiss NTS GMBH, Germany, SUPRA 55. TEM analysis was performed using Transmission electron microscope CM 200 (Philips).

For electrical measurements, impedance spectroscopy was performed on sintered pellets of four samples CE, CG2, CG4 and CG6. The pellets were made by pressing 4 g of powder at 200 MPa in a 25 mm die and were sintered for 6 hours at the temperatures 1150°C and 1250°C. The densities of pellets pressed and sintered at 1250°C for 6 h as described above were determined from their mass and dimensions. For electrical measurements, silver contacts were applied on both the flat surfaces and cured at 500°C for 15 min. An impedance analyzer (KEYSIGHT-E4990A) was used to characterize the impedance spectra of sintered samples in the static ambient atmosphere in the frequency range 20 Hz to 5 MHz from 550 to 950°C. The spectra were fitted using the Zsimpwin software and values for the total, bulk and grain boundary conductivities were noted.

4. Result and discussion

4.1 XRD analysis

Structural Analysis Figure 1 shows the XRD pattern of the prepared cerium oxide sample. All the diffraction peaks of (111) at 28.64°, (200) at 33.27°, (220) at 47.76°, (311) at 56.78°, and (400) at

69.10° were indexed and well matched with standard JCPDS Card No. 65-5923. The patterns of cerium oxide samples confirmed the cubic structure of the material. The sharp and high intense peaks of XRD patterns confirm the high crystalline quality of the samples. The crystallite size of pure cerium oxide was calculated from the diffraction peaks of XRD pattern using Scherer's formula. The average crystallite size was calculated using Scherrer equation were calculated from (111) peak and are presented in Table 1. The size of Gd doped CeO_2 nanoparticles decreased with increasing the concentration of Gd. The average crystallite size of the crystals was found in between 43-45 nm with slight expansion of lattice. The crystallinity of the powder became better during the calcination at 550°C. Crystalline phases corresponding to Gd_2O_3 could not be found for as-prepared powders, indicating the formation of solid solution. A trivial expansion in the lattice constant upon doping has been attributed to the substitution of the smaller Ce^{4+} ion (0.97Å) by the larger Gd^{3+} (1.053Å) ions, which caused strain and as light deformation no the structure. The introduction of Gd^{3+}, ions into Ce^{4+} can cause a small shift in the cerium oxide peaks positions. Since the broadening of peaks could be attributed not only to crystallite size, but also to stresses created in the structure.
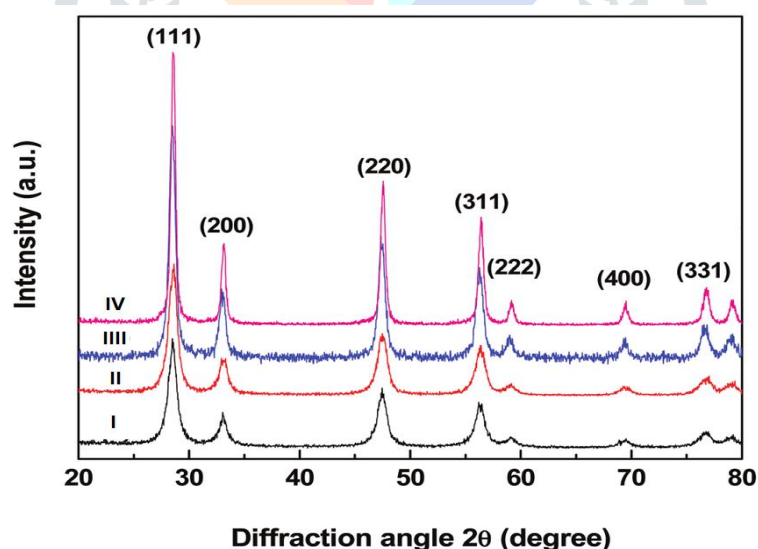

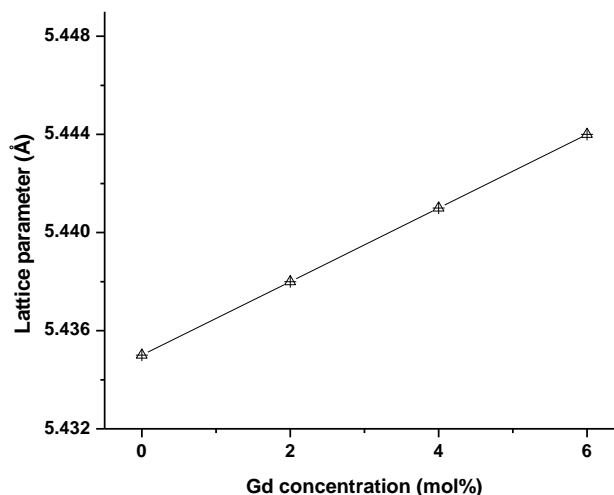**Figure (1) XRD patterns of Gd doped CeO_2 powders obtained at 550°C.**

Figure (2) Plot against Gd concentration (mol%) for lattice parameter of as-prepared ceria-based materials.

Table (1) 2θ (deg.), crystallite size (nm) and d-spacing of pure and Gd-doped CeO$_2$ nanoparticles.

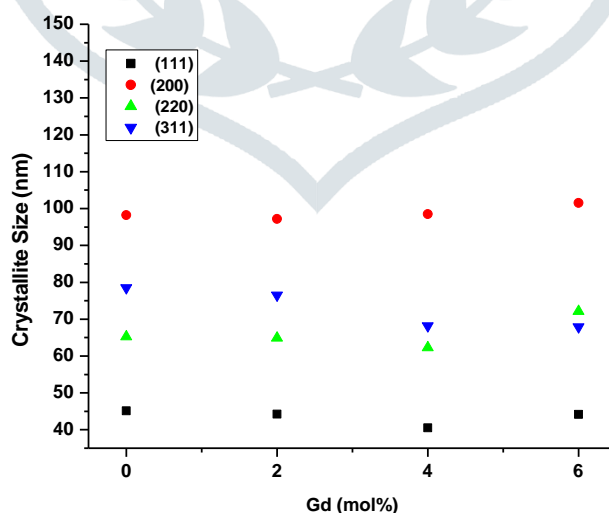| Sample	Gd (mol%)	2 Theta (deg.)	Crystallite size (nm)	*d*-spacing	*Band Gap (eV)*
C	0.0	28.51	45.15	3.134	2.78
CG2	2	28.49	44.24	3.132	2.65
CG4	4	28.47	42.58	3.130	2.49
CG6	6	28.44	44.17	3.130	2.54

Figure (3) 3.2 Crystal growth as a function of Gd concentration.

Observed results are summarized and compared for better illustration in Figure 3. While the crystal growth was slow until reaching 4 mol% of Gd, at higher concentration the crystal growth was much faster.

4.2 FTIR spectra

Fourier transform infrared (FTIR) spectra of the as-prepared Gd-doped nanocomposites are shown in Figure 4. Some distinctive absorptions peaks were observed at 3436 and 1630 cm^{-1}. Two strong intense bands observed at 3429 and 1624 cm^{-1} of pure and Gd-doped CeO_2 samples are attributed to (O–H) vibration modes of (H-bonded) water molecules, which was due to the physically observed water on the sample surfaces [38, 39]. The strong band at 3429 cm^{-1} is attributed to the v (O–H) vibration modes of the water molecules adsorbed physically. In addition, some weaker absorption peaks were also observed at around 2934, 2856, 1369, 1092, and 700 cm^{-1}. The bands observed at 2934 and 2856 cm^{-1} are due to the (C–H) bonds of organic molecules absorbed during the sample preparation and handling [40]. Absorption at 1630 cm^{-1} is assigned to a systematic stretching vibration of the carboxylate (-COO−) group [17]. The peak at around 1092 cm^{-1} indicates the presence of the nitrate ions [18]. The bands observed in the lower frequency region at 700 and 430 cm^{-1} are referred to the characteristic Ce–O vibration [19]. The band at 1369 cm^{-1} is assigned to the stretching vibration of carboxylate salts (COO^{-}) [41, 42]. The band observed at 1092 cm^{-1} due to the Cerium- Oxygen group with a larger double bond nature [43]. Two weaker bands observed at 852 and 735 cm^{-1} are due to Cerium-Oxygen group having a lower double bond nature and of Ce–O–Ce chains asymmetric stretching vibration of metal oxide networks respectively. The strong band noticed at 558 cm^{-1} is due to the symmetrical stretching vibration mode of (Ce–O–Ce) or (Ce–O–Gd) indicating the Gd ions doped Ceria nanoparticles [44]. It is to be noted that the length of the rare-earth metals-oxygen bond changes with dopant concentration. These shifts in peaks confirm the dopant stabilization in the host lattice [45].
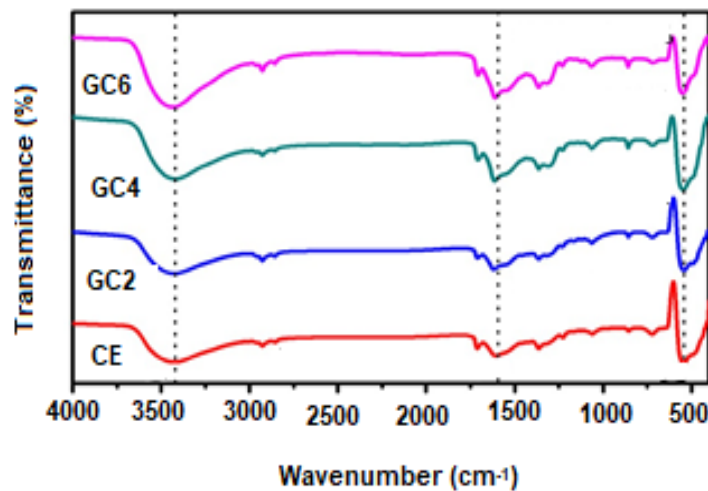
Figure (4) FTIR spectra of Gd-doped Ceria nanocomposites.

4.3 UV-VIS studies

The UV-VIS spectroscopic measurement was carried out to investigate the effect of Gd concentration on the optical properties of CeO_2 nanocomposites. Figure 5 shows the UV-VIS absorption spectra recorded for pure and Gd-doped ceria. It can be seen that there is a strong absorption band below 400 nm in the spectra for all the samples, which is due to the charge transfer from O^{-2} (2p) to Ce^{4+}(4f) orbitals in CeO_2 [46]. The optical band gap values for the Gd-doped ceria system can be estimated from the absorption spectra following Tauc's equation [47].

$$\alpha h v = A\left(h v - E_g\right)^n$$

where α is the absorption co-efficient, hv is the photon energy, E_g is the band gap energy, A is a constant and n can have values of 1/3, 1/2, 2, and 3 for the direct forbidden, direct allowed, indirect allowed, and indirect forbidden transitions respectively. The calculated values of E_g for all the as-prepared samples are given in Table 1 Undoped ceria shows the highest band gap value of 2.79 eV, and for Gd-doped ceria the values of the band gap decrease with the Gd concentration. Thus, the absorption spectra of Gd^{3+} doped ceria nanocrystals exhibit red shifts compared to that of pure ceria.
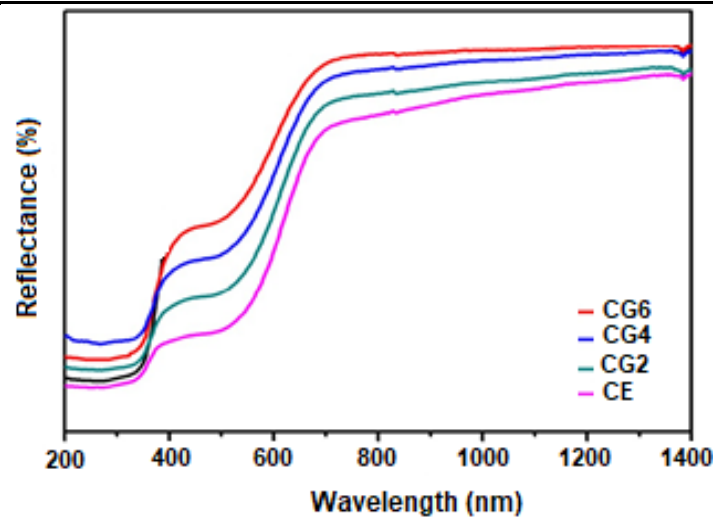
Figure (5) UV-VIS spectra of Gd-doped Ceria nanocomposites.

In CeO_2, all valance Ce states, including the 4f states, are empty, and the system is a wide gap insulator with a measured fundamental band gap of 6.0 eV between the valance and conduction bands; this is formed predominantly by the O^{-2} (2p) to Ce^{4+} (5d) states respectively [48]. However, in our present study, the band gap value of CeO_2 is much lower than 6.0 eV (Table 1). This is because a small amount of Ce^{3+} is present at the surface of CeO_2 and one electron per Ce atom populates a Ce 4f state, resulting in a decrease in the band gap value of ceria [49]. The red shift of the direct band gap may be due to the presence of oxygen defect levels between the O2p and Ce4f levels that capture the excited electrons and decrease the effective band gap [50]. Lastly, the doping of Gd ions creates ground and excited f-energy states in the mid band gap of ceria. These energy states of Gd accept many of the excited electrons coming from the O2p level which leads into the effective reduction in the band gap., i.e. a red shift [51].

4.4 SEM and EDS spectra

The effect sintering temperature on morphology and density cannot be predicted by preliminary analyses because at a comparable density, the microstructure is completely different as visible in Figure 6. At sintering temperatures of 1150 and 1250°C, pure electrolytes have small grains with a similar uneven and rough morphology. These samples are affected by the poorest densification with an inadequate microstructure for the lowest sintering temperatures. By increasing temperature. The microstructure is always revealing small grains, many cracks, and voids, but the morphology became more uniform, and the relative density increases. The addition of Gd, make obvious a change in the

microstructure according to sintering temperature. As reported for sample GC4 in Figure 6 microstructure with clean grain boundaries was formed at 1250°C.

Figure 6 shows SEM micrographs of sintered GC4 samples and EDS analysis of the Gd_2O_3 doped CeO_2 crystals. The average size and size distribution of the synthesized particles were below 10 nm and uniform, respectively. The shape of the synthesized particles was nearly spherical. The spectrum of Gd_2O_3 doped CeO_2 nanoparticles according to a SEM - EDS analysis. The particles show Gd, Ce and O pattern peaks Table 2.
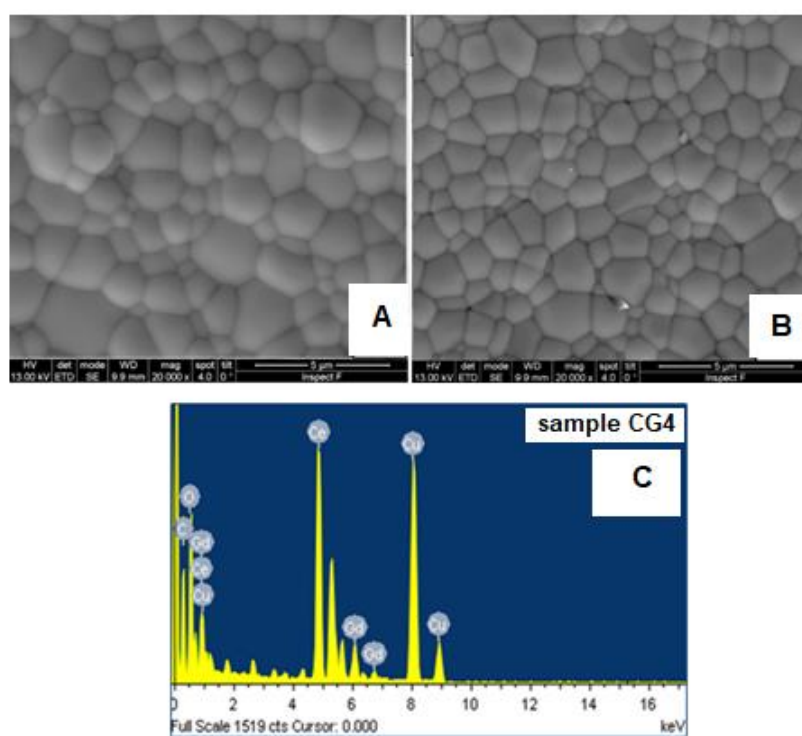

Figure (6) SEM of sample GC4 sintered at (A) 1150°C and (B) 1250°C   (C) EDAX spectra of sample GC4.

Table (2) Elemental composition obtained for EDS spectroscopy.

Element	Weight (%)	Atomic (%)
C K	7.20	29.37
O K	10.21	31.37
Cu K	24.63	19.08
Ce K	53.06	18.64
Gd K	4.96	1.55
Total	100.00	

4.5 Electrical Properties

The total resistance (R_T) of as-prepared sample can be obtained by utilizing the impedance spectroscopy at different temperatures. The total electrical conductivity σ_T was then calculated according to the equation,

$$R_T = R_{grain} + R_{grain-boundary} \tag{1}$$

The total electrical conductivity (σ_T) was then determined from the following equation –

$$\sigma = \frac{l}{AR_T} \tag{2}$$

where, l is the thickness and A represents the cross-sectional area of the sample. It is reported that, the conductivity of ceria-based electrolytes in air is based on ionic conductivity and the contribution of electronic conductivity is negligible [52]. In this study, the conductivity of as-prepared samples measured in air was treated as the oxide ionic conductivity only. The ionic conductivity (σ_t) in ceria-based oxides is a temperature dependent and it can be expressed by the following empirical relationship –

$$\sigma_t T = \sigma_o \exp\left(\frac{E_a}{kT}\right) \tag{3}$$

where E_a is the activation energy for conduction, T is the absolute temperature, k is the Boltzmann constant and σ_0 is a pre-exponential factor. The equation can be linearised by plotting a logarithmic relationship between $\log(\sigma_t T)$ and 1000/T (K).
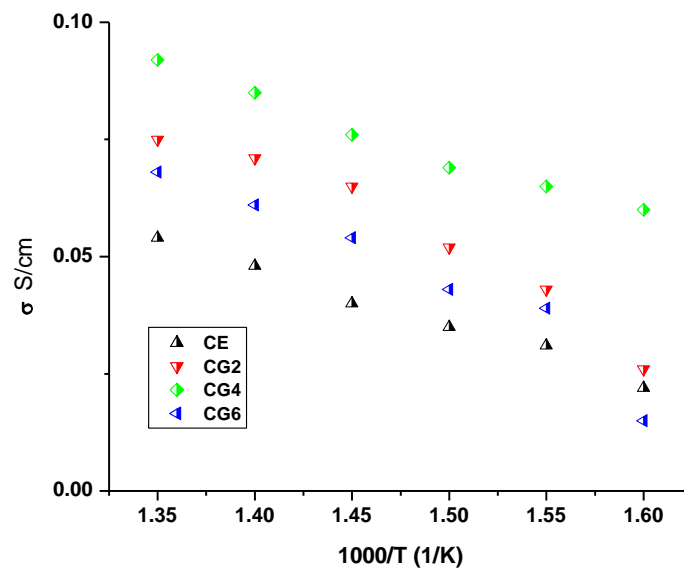
Figure (7) Ionic conductivity of as prepared Gd-doped ceria nanocomposites at different operational
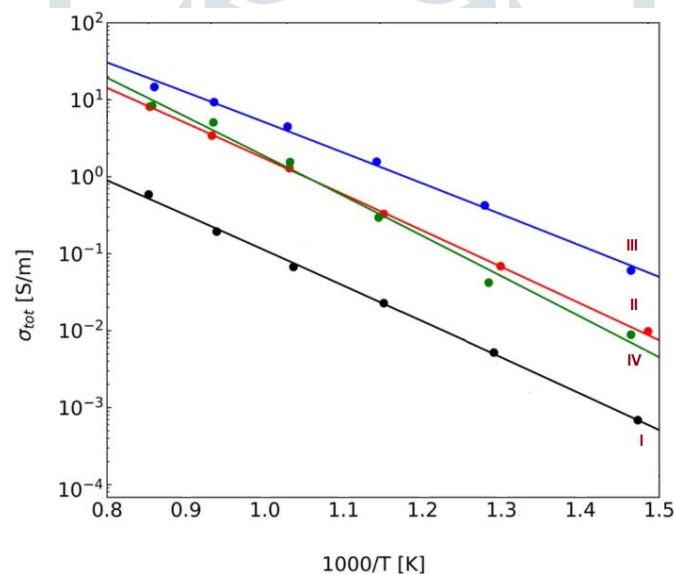
temperatures.

Figure (8) Arrhenius plot of ionic conductivity for (I) sample Ce, (II) sample CG2, (III) sample CG4 and

(IV) sample CG6.

The Arrhenius plot of ionic conductivity for different dopant concentrations is presented in Figure 8. The plots clearly reveal a linear increase of conductivity with temperature. Conductivity for pure ceria is lowest and tends to increase with Gd concentration up to a maximum at 4 mol% (sample CG4) and when Gd concentration is 6mol%, the conductivity is found to be declined. Conductivity of CG2 is slightly higher than CG6. The activation energy of ionic conductivity calculated from Arrhenius plot are obtained as 0.84 eV, 0.98 eV, and 1.15 eV for CG4, CG2, and for pure-ceria (CE),

respectively; the activation energy of GDC is comparable with reported values [52-58]. The change in the activation energy may be attributed to an order and disorder transition of the oxygen sublattice caused due to successful substitution of Ce^{4+} ions by Gd^{3+} ions [59]. The activation energy is minimum for the SDC. This decrease in activation energy may be due to the presence of attractive interactions between dopant cations and oxygen vacancies [60]. Moreover, an increase in the Gd concentration in the ceria structure, dopant process hinders oxygen arrangement causing an increase in the activation energy and a decrease in the ionic conductivity for the ceria solid solutions. At lower temperatures, the activation energy (E_a) depends on the defect association enthalpy (ΔH_a) and migration enthalpy (ΔH_m) for conduction. At higher temperatures, activation energy is equal to only the migration enthalpy (ΔH_m), because a great part of the oxygen vacancies is free to diffuse [61].

The appearance of high oxygen ionic conductivity in the solid electrolytes is determined by the formation of oxygen vacancies in the CeO_2 matrix when Ce^{4+} is replaced by Gd^{3+} during the dissolution of Gd_2O_3 in the lattice of CeO_2, which can be described by the following quasi-chemical equation [3].

$$Gd_2O_3 \xrightarrow{Ce_2O_3} 2Gd'_{Ce} + 3O_O^X + V_O^{\cdot\cdot}$$

Where Gd'_{Ce} is a Gd^{3+} ion replacing Ce^{4+} and yielding a negative charge, $V_O^{\cdot\cdot}$ is a positively charged oxygen vacancy compensating the dopant charge, O_O^X is oxygen atom in a regular site with a neutral charge. It was observed that, increased temperature in the range from 570 to 970°C leads to the increase in electrical conductivity of all the samples. In addition, with an increase in the concentration of Gd_2O_3, the specific electrical conductivity of the ceramics increases in the entire temperature range in study. The highest specific electrical conductivity in the temperature range of 550–950°C ($\sigma_t = 3.3 \times 10^{-2}$ Scm^{-1} at 750°C) is observed for the sample CG4 containing 4 mol.% Gd_2O_3.

Table (3) Total ionic conductivity of Nd-doped CeO_2 solid solutions at 750°C.

Sample	Total Ionic Conductivity (Scm^{-1})	Activation energy (eV)
CE	1.02×10^{-6}	0.79
GC2	2.34×10^{-4}	0.87
GC4	3.3×10^{-2}	0.71
GC6	1.43×10^{-3}	0.87

It has been observed that the activation energy decreases with a rise in the dopant concentration as shown in Table 3. The contribution of grain conductivity is a major factor for the total oxide ion conductivity in the doped ceria samples [62]. Thus, the amount of Gd doping affects the conductivity of the ceria. With the ascent in the Gd concentration, a huge expansion in the grain conductivity was seen because of the improvement of the charge transporters emerging from the creation of oxygen vacancies as a result of doping. This leads into the expansion of the crystal structure.

5. Conclusion

The Gd-doped ceria nanocomposites with composition $Ce_{1-x}Gd_xO_{2-\delta}$ (x = 0.0, 2.0, 4.0 and 6.0wt%) were successfully prepared by using a EDTA-glycol method. The XRD, FTIR, UV-visible, SEM–EDS analysis confirmed the formation of the single-phase solid solution. All as-prepared Gd-doped ceria nanocomposites were sintered at the temperatures 1150 and 1250°C. The nanocomposite containing 4wt% Gd showed an essentially upgraded oxide ion conductivity in the order of 3.3×10^{-2} Scm^{-1} at 750°C with a lower activation energy, E_a = 0.71 eV. Thus, Gd-doped ceria nanocomposites might be viewed as a potential electrolyte material for SOFC applications.

6. References

[1] Subotić, V.; Napporn, T.W. Nanostructured metal oxides for high-performance solid oxide fuel cells (SOFCs). In *Metal Oxide-Based Nanostructured Electrocatalysts for Fuel Cells, Electrolyzers, and Metal-Air Batteries*; Napporn, T.W., Holade, Y., Eds.; Elsevier: Amsterdam, The Netherlands, **2021**; pp. 235–261.

[2] Choolaei, M.; Cai, Q.; Horri, B.A. Green synthesis and characterization of nanocrystalline NiO-GDC powders with low activation energy for solid oxide fuel cells. *Ceram. Int.* **2021**, *47*, 32804–32816.

[3] Liang, J. Low temperature fabrication of dense gadolinia-doped ceria electrolyte with enhanced electrical conductivity. Electrochim. Acta **2015**, 178, 321–328.

[4] Rekas, M. Electrolytes for Intermediate Temperature Solid Oxide Fuel Cells. Arch. Met. Mater. **2015**, 60, 891–896.

[5] Mahato, N.; Banerjee, A.; Gupta, A.; Omar, S.; Balani, K. Progress in material selection for solid oxide fuel cell technology: A review. Prog. Mater. Sci. **2015**, 72, 141–337.

[6] Sal'Nikov, V.V.; Pikalova, E.Y. Raman and impedance spectroscopic studies of the specific features of the transport properties of electrolytes based on CeO. Phys. Solid State 2015, 57, 1944–1952.

[7] Egorova, T.L.; Kalinina, M.V.; Simonenko, T.; Shilova, O.A.; Sevastyanov, V.G.; Kuznetsov, N.T. Liquid-phase synthesis and physicochemical properties of xerogels, nanopowders and thin films of the CeO_2–Y_2O_3 system. Russ. J. Inorg. Chem. 2016, 61, 1061–1069.

[8] Egorova, T.L.; Kalinina, M.V.; Simonenko, T.; Shilova, O.A.; Sevastyanov, V.G.; Kuznetsov, N.T. Liquid-phase synthesis and physicochemical properties of xerogels, nanopowders and thin films of the $CeO2$–$Y2O3$ system. Russ. J. Inorg. Chem. **2016**, 61, 1061–1069.

[9] Ramos-Alvarez, P.; Villafuerte-Castrejón, M.E.; González, G.; Cassir, M.; Flores-Morales, C.; Chávez-Carvayar, J.A. Ceria-based electrolytes with high surface area and improved conductivity for intermediate temperature solid oxide fuel cells. J. Mater. Sci. **2016**, 52, 519–532.

[10] Steele B C H **2000** Solid State Ionics 1343.

[11] Arachi Y, Sakai H, Yamamoto O, Takedsa Y and Imanishai **N1999** Solid State Ionics 121133.

[12] Eguchi K, Setoguchi T, Inoue T and Arai H **1992** Solid State Ionics 52165

[9] Mogensen M, Sammes N M and Tompsett GA **2000** Solid State Ionics 12963.

[10] Zha S, Xia C and Meng G **2003** J. Power Sources 11544.

[11] Fuentes R O and Baker R T **2008** Int. J. Hydrogen Energy 33 3480.

[12] Namitha R, Radhika D, Krishnamurthy G (**2019**) Hydrothermally synthesized carbon nanotubes for electrochemical hydrogen storage application. Issues Chem Chem Technol 3:30–34.

[13] Dell'Agli G, Spiridigliozzi L, Pansini M, Accardo G, Yoon SP, Frattini D (**2018**) Effect of the carbonate environment on morphology and sintering behaviour of variously co-doped (Ca, Sr, Er, Pr) Samarium-doped ceria in co-precipitation/hydrothermal synthesis. Ceram Int 44:17935–17944.

[14] Ghelich R, Keyanpour-Rad M, Youzbashi AA, Khakpour Z (**2015**) Comparative study on structural properties of NiO–GDC nanocomposites fabricated via electrospinning and gel combustion processes. Mater Res Innov 19:44–50.

[15] Arabaci A (**2018**) Synthesis and characterization of Pr/Gd co-doped ceria by using the citric acid–nitrate combustion method. Solid State Ionov 326:69–76.

[16] Radhika D, Kannan K, Nesaraj AS, Namitha R (**2019**) Facile low-temperature synthesis and application of $La_{0.85}Sr_{0.15}Co_{0.85}Fe_{0.15}O_{3-\delta}$ as superior cathode for LT-SOFCs Using C-TAB as surfactant. Mater Res Innov 10:12.

[17] Radhika Devi, Nesaraj AS (**2014**) Chemical precipitation and characterization of multicomponent perovskite oxide nanoparticles—possible cathode materials for low temperature solid oxide fuel cell. Int J Nano Dimension 5:1–10.

[18] Chaubey, N.; Wani, B.N.; Bharadwaj, S.R.; Chattopadhyaya, M. C. Physicochemical properties of rare earth doped ceria $Ce0.9Ln0.1O1.95$ (Ln = Nd, Sm, Gd) as an electrolyte material for IT-SOFC/SOEC. Solid State Sci. 2013, 20, 135–141.

[19] Yahiro, H.; Eguchi, K.; Arai, H. Electrical properties and reducibilities of ceria-rare earth oxide systems and their application to solid oxide fuel cell. Solid State Ion. 1989, 36, 71.

[20] Anirban, S. K. Dutta, A. Revisiting ionic conductivity of rare earth doped ceria: Dependency on different factors. Int. J. Hydrogen **2020**, 45, 25139.

[21] Huang, W.; Shuk, P.; Greenblatt, M. Properties of sol-gel prepared $Ce_{1-x}Sm_xO_{2-x2}$ solid electrolytes. Solid StateIon.**1997**,100,23.

[22] Yahiro, H.; Eguchi, Y.; Eguchi, K.; Arai, H. Oxygen ion conductivity of the ceria-samarium oxide system with fluorite structure. J. Appl. Electrochem.**1988**,18,527.

[23] Arabaci, A. Effect of Sm and Gd dopants on structural s characteristics and ionic conductivity of ceria. Ceram. Int.**2015**,41,5836.

[24] Steele, B. C. H. Appraisal of $Ce_{1-y}Gd_yO_{2-y/2}$ electrolytes for IT-SOFC operation at 500°C. Solid StateIon.**2000**,129,95.

[25] Butler, V.; Catlow, C.; Fender, B.; Harding, J. Dopant ion radius and ionic conductivity in cerium dioxide. Solid StateIon.**1983**, 8,109.

[26] H. Inaba, H. Tagawa, Solid State Ionics 83 (**1996**) 1−16.

[27]. K. Eguchi, T. Setoguchi, T. Inoue, H. Arai, Solid State Ionics 52 (**1992**) 165−172.

[28] T. Mori, Z. Li, P. Yan, Y. Wu, Z. Li, Mater. Sci. Eng. B 177 (**2012**) 1538−1541.

[29]. T. Mori, J. Drennan, J.H. Lee, J.G. Li, T. Ikegami, Solid State Ionics 154−155 (**2002**) 461−466.

[30]. V.V. Kharton, F.M.B. Marques, A. Atkinson, Solid State Ionics 174 (**2004**) 135−149.

[31] K.C. Anjaneya, J. Manjanna, G. Govindaraj, K.N. Ganesha, J. Alloys Compd. 578 (**2013**) 53−59.

[32] L.D. Jadhav, M.G. Chourashiya, A.P. Jamale, A.U. Chavan, S.P. Patil, J. Alloys Compd. 506 (2010) 739−744.

[33]. R.K. Lenka, T. Mahata, A.K. Tyagi, P.K. Sinha, Solid State Ionics 181 (**2010**) 262−267.

[34]. K.C. Anjaneya, J. Manjanna, G. Govindaraj, K.N. Ganesha, J. Alloys Compd. 585 (**2014**) 594−601.

[35]. K.C. Anjaneya, J. Manjanna, G. Govindaraj, K.N. Ganesha, Physica B 447 (**2014**) 51−55.

[36]. T. Karaca, T.G. Altmcekic, M.F. Oksuzomer, Ceram. Int. 36 (**2010**) 1101−1107.

[37]. S. Li, L. Ge, H. Gu, Y. Zheng, H. Chan, L. Guo, J. Alloys Compd. 509 (**2011**) 94−98.

[38]. J. Chandradass, B. Nam, K.H. Kim, Colloids Surf. A 348 (**2009**) 130−136.

[39] S. Samiee, E.K. Goharshadi, Effects of different precursors on size and optical properties of ceria nanoparticles prepared by micro- wave-assisted method. Mater. Res. Bull. **47**, 1089–1095 (2012).

[40] G. Wang, Q. Mu, T. Chen, Y. Wang, Synthesis, characterization and photoluminescence of CeO_2 nanoparticles by a facile method at room temperature. J. Alloy. Compd. **493**, 202–207 (2010).

[41] S. Phoka, P. Laokul, E. Swatsitang, V. Promarak, S. Seraphin, S. Maensiria, Synthesis, structural and optical properties of CeO_2 nanoparticles synthesized by a simple polyvinyl pyrrolidone (PVP) solution route. Mater. Chem. Phys. **115**, 423–428 (2009).

[42] A.Z. Liu, J.X. Wang, C.R. He, H. Miao, Y. Zhang, W.G. Wang, Synthesis and characterization of $Gd_{0.1}Ce_{0.9}O_{1.95}$ nanopowder via an acetic-acrylic method. Ceram. Int. **39**, 6229–6235 (2013).

[43] R. Tholkappiyan, A. Nirmalesh Naveen, S. Sumithra, K. Vishista, Investigation on spinel $MnCo_2O_4$ electrode material prepared via controlled and uncontrolled synthesis route for supercapacitor application. J. Mater. Sci. **50**, 5833–5843 (2015).

[44] C. Binet, A. Badri, J.C. Lavalley, A spectroscopic characterization of the reduction of ceria from electronic transitions of intrinsic point defects. J. Phys. Chem. **98**, 6392–6398 (1994).

[45] C. Ho, J.C. Yu, T. Kwong, A.C. Mak, S. Lai, Morphology-control- lable synthesis of mesoporous CeO₂ nano- and microstructures. Chem. Mater. **17**, 4514–4522 (2005).

[46] R. Tholkappiyan, K. Vishista, Synthesis and characterization of barium zinc ferrite nanoparticles: working electrode for dye sen‑sitized solar cell applications. Sol. Energy **106**, 118–128 (2014).

[47] Y.-W. Zhang, R. Si, C.-S. Liao, C.-H. Yan, C.-X. Xiao and Y. Kou, J. Phys. Chem. B, 2003, 107, 10159–10167.

[48] S. L. S. Rao, G. Ramdevudu, Md. Shareefuddin, A. Hameed, M. N. Chary and M. L. Ro, Int. J. Eng. Sci. Res. Technol., 2012, 4, 25–35.

[49] 5 E. Wuilloud, B. Delley, W. D. Schneider and Y. Baer, Phys. Rev. Lett., 1984, 53, 202–205.

[50] L. Wu, H. J. Wiesmann, A. R. Moodenbaugh, R. F. Klie, Y. Zhu, D. O. Welch and M. Suenaya, Phys. Rev. B: Condens. Matter Mater. Phys., 2004, 69, 125415.

[51] A. H. Morshed, M. E. Moussa, S. M. Bedair, R. Leonard, S. X. Liu and N. El-Masry, Appl. Phys. Lett., 1997, 70, 1647– 1649.

[52] M. Greenberg, E. Wachtel, I. Lubomirsky, J. Fleig and J. Maier, Adv. Funct. Mater., 2006, 16, 48–52.

[53] M. G. Chourashiya, S. R. Bharadwaj, and L. D. Jadhav, Thin Solid Films 519, 650 (2010).

[54] S. L. Reis, E. C. C. Souza, and E. N. S. Muccillo, Solid State Ionics 192, 172 (2011).

[55] H. Duncan and A. Lasia, Solid State Ionics 176, 1429 (2005).

[56] D. Perez-Coll, P. Nu~nez, J. C. Ruiz-Morales, J. Pe~na-Martınez, and J. R. Frade, Electrochim. Acta 52, 2001 (2007).

[57] A. Jasper, J. A. Kilner, and D. W. McComb, Solid State Ionics 179, 904 (2008).

[57] S. Dikmen, H. Aslanbay, E. Dikmen, and O. S¸ahin, J. Power Sources 195, 2488 (2010).

[58] G. Kim, N. Lee, K. B. Kim, B. K. Kim, H. Chang, S. J. Song, and J. Y. Park, Int. J. Hydrogen Energy 38, 1571 (2013).

[59] H. Inaba, H. Tagawa, Ceria-Based Solid Electrolytes, Solid State Ion. 83, 1 (1996).

[60] K. Zhao and Y. Du, Calcium-doped ceria materials for anode of solid oxide fuel cells running on methane fuel, *J. Power Sources*, 2017, 347, 79.